8. Ocean Electromagnetics

John J. Holmes

Even though acoustic waves can travel long distances in the sea with little attenuation, ocean electromagnetics has important applications in the areas of geophysical surveys and searches of the seafloor and sub-bottom, communications across the sea–air boundary, and high data transfer rate at short ranges. Unlike in-air propagation of electromagnetic fields, the finite conductivity of seawater results in a frequency-dependent phase velocity, attenuation, intrinsic impedance, and reflection and transmission coefficients at the ocean's surface. After giving a short summary of the electric and magnetic properties of the ocean, this chapter begins with Maxwell's equations and develops the mathematical descriptions of electromagnetic fields and dipole sources within a conducting media. The differences between plane wave reflection and transmission at the surface of fresh water and seawater are used to highlight how electromagnetic propagation within the electrically conducting ocean is so very different than the more familiar radio frequency transmissions in air. In addition, equations are presented that describe the fields from submerged electric and magnetic dipoles that are located both far and near the sea surface. These formulations are valid over the frequency range from 0 Hz to a few MHz. Finally, a brief discussion of ocean electromagnetics at optical wavelengths is given at the end of this chapter.

Even though acoustic waves can travel long distances in the sea with little attenuation, ocean electromagnetics has several important applications. For example; electromagnetic surveys, searches, and communication systems can operate effectively in acoustically noisy environments, they can cross the sea–air boundary and be received by high speed airborne sensors, and they have much higher data transfer rates at short ranges. In addition, electromagnetic surveys of seafloor gas hydrate pockets can determine their methane content, a shortfall of seismic techniques. Moreover, the short range limitations of underwater electromagnetic field propagation are actually beneficial when pinpointing submerged targets during naval operations.

8.1 Electromagnetism in an Ocean Environment

The oldest known application of electromagnetism in an ocean environment is the magnetic compass used for navigation. Today, electromagnetic sources and sensors are useful tools found in many diverse areas of oceanographic study such as physical oceanography, seafloor geophysics, marine chemistry, and biology. Advances in the understanding of electromagnetism within the boundaries of these scientific disciplines have found application to engineering systems for energy generation, oil and gas exploitation and recovery, commercial fishing, weather prediction, Tsunami warning, archeology, and the military. This chapter will

present a brief description of the science behind electromagnetic fields and their interaction with an ocean environment.

Pure water is a very good dielectric. Its *permittivity* is given by $\varepsilon = \varepsilon_0 \varepsilon_w$, where ε_0 is the free-space permittivity ($\approx 8.8541878176 \times 10^{-12}$ F/m), and ε_w is the water's dielectric constant equal to approximately 80.1 at 20 °C. Due to the strong covalent bonds of the hydrogen and oxygen atoms in the water molecule, there are no electrons in the conduction band until they are pumped up to that energy level by applying high amplitude electric fields. If the field reaches a few megavolts/cm, pure water will undergo a dielectric *breakdown* forming an electric arc in the process. Although pure water is a very good insulator, seawater is a good electric conductor.

The disassociated salt ions in seawater cause it to be a good electric conductor at all field levels. Although electrons are the primary charge carriers in metallic conductors, the positively charged salt ions, called *cations* and negatively charged *anions*, are both charge carriers in seawater. If a source of electric potential gradient is introduced into the seawater, the cations will migrate toward the source's *cathode* (negative pole), while the anions travel toward the *anode* (positive pole). Electrochemical reactions occur at the anode, releasing electrons in the process that then flow in the source's metallic conductor to the cathode where they recombine with the cations.

The mobility of seawater ions is hampered by their interaction with water molecules as they migrate, resulting in loss of energy in the form of heat. At the engineering level, seawater can be treated as a simple conductor with an *electric conductivity* σ ranging from about 2.5 S/m in cold deep waters, and approaches 6 S/m in very warm waters. (A value of 4 S/m is typically used for open ocean seawater.) This finite conductivity attenuates electromagnetic energy as it propagates through seawater, which is categorized as a lossy medium.

Fortunately, seawater is nonmagnetic. Its *magnetic permeability* is the same as free-space given by $\mu_0 = 4\pi 10^{-7}$ H/m. This means the only way that seawater can be a source of a static magnetic field is by electric current flowing through it.

This chapter will focus on the science of electromagnetic field propagation and attenuation in seawater, and the reflection and transmission of the fields at the sea's surface. Emphasis will be placed on electromagnetic field theory in the ultralow frequency (ULF) band of ≈0 to 3 Hz, and the extremely low frequency (ELF) band from 3 Hz to 3 kHz. Since the attenuation of electromagnetic waves increases rapidly with frequency, radio frequency bands will not be covered here. Although remote observations of the sea surface from airborne and satellite-based microwave radiometers and radars are important tools for oceanographic research, they are beyond the scope of this discussion. (The interested reader should consult [8.1, pp. 405–510] on this topic.) A brief cursory discussion of ocean electromagnetics at optical wavelengths will be given at the end of this chapter.

8.2 Electromagnetic Field Theory

It is not possible to give an in-depth description of general electromagnetic field theory here. A comprehensive treatment of engineering electromagnetics is presented in [8.2]. In order to introduce some basic principles for electromagnetic fields in a lossy media such as seawater, the formulations for magnetic and electric fields in an unbounded ocean will be presented first.

All electromagnetic field theories are based on *Maxwell's equations*. In differential form, they are

$$\nabla \times \boldsymbol{E} = -\frac{\partial \boldsymbol{B}}{\partial t}\,, \tag{8.1}$$

$$\nabla \times \boldsymbol{H} = \boldsymbol{J} + \frac{\partial \boldsymbol{D}}{\partial t}\,, \tag{8.2}$$

$$\nabla \cdot \boldsymbol{D} = q_e\,, \tag{8.3}$$

$$\nabla \cdot \boldsymbol{B} = 0\,, \tag{8.4}$$

where $\boldsymbol{E}$ (v/m) and $\boldsymbol{H}$ (A/m) are the electric and magnetic field *intensity vectors*, $\boldsymbol{D}$ (c/m^2) and $\boldsymbol{B}$ (wb/m^2 or T) are the electric and magnetic *flux density vectors*, $\boldsymbol{J}$ (A/m^2) is the electric *current density*, q_e (c/m^3) represents the *electric charge density*, and t stands for time (seconds). Maxwell's equations by themselves are sufficient to solve any problem in electromagnetics.

Although magnetic charge and magnetic current densities are not realizable, they can be included in Maxwell's equations through the *generalized* current concept to aid mathematically in the solutions of certain problems. For example, a magnet can be represented mathematically as two opposite polarity magnetic charges at its ends. Adding the virtual magnetic sources to Maxwell's equations, and separating the current density into its impressed and conduction components, allows (8.1) through (8.4) to be written in a more symmetrical form as

$$\nabla \times \boldsymbol{E} = -\boldsymbol{M}_i - \frac{\partial \boldsymbol{B}}{\partial t}\,, \tag{8.5}$$

$$\nabla \times \boldsymbol{H} = \boldsymbol{J}_\mathrm{i} + \boldsymbol{J}_\mathrm{c} + \frac{\partial \boldsymbol{D}}{\partial t} , \tag{8.6}$$

$$\nabla \cdot \boldsymbol{D} = q_\mathrm{e} , \tag{8.7}$$

$$\nabla \cdot \boldsymbol{B} = q_\mathrm{m} , \tag{8.8}$$

where $\boldsymbol{M}_\mathrm{i}$ $(\mathrm{v/m^2})$ is the *impressed magnetic current density*, $\boldsymbol{J}_\mathrm{i}$ $(\mathrm{A/m^2})$ is the *impressed electric current density* produced by an active source, $\boldsymbol{J}_\mathrm{c}$ is the *conduction current* density flowing in the media, and the equivalent *magnetic charge density* is represented as q_m $(\mathrm{wb/m^3})$. The symmetric form of Maxwell's equations, (8.5) through (8.8), will be used here.

The electromagnetic properties of seawater are very different than air or free space. As a result, the interaction of electromagnetic fields with the ocean is unlike that in air. The relationships between the field intensities and flux densities are related by the *constitutive parameters* of the media as given by

$$\boldsymbol{B} = \mu \boldsymbol{H} , \tag{8.9}$$

$$\boldsymbol{D} = \varepsilon \boldsymbol{E} , \tag{8.10}$$

$$\boldsymbol{J} = \sigma \boldsymbol{E} , \tag{8.11}$$

where μ, ε, and σ for seawater have been defined previously. In air, $\mu = \mu_0$, $\varepsilon = \epsilon_0$, and $\sigma = 0$.

Continuity of electric charge is an important relationship that can be derived from Maxwell's equations. The *continuity equation* is given by

$$\nabla \cdot \boldsymbol{J} = -\frac{\partial \rho}{\partial t} . \tag{8.12}$$

This expression relates how the charge in a volume changes with the current density entering or leaving it.

The first two Maxwell's equations, (8.5) and (8.6), are a set of first-order differential equations that are coupled. The first step in their solution is to uncouple them. Using (8.9)–(8.11) to rewrite (8.5)–(8.8) gives

$$\nabla \times \boldsymbol{E} = -\boldsymbol{M}_\mathrm{i} - \mu \frac{\partial \boldsymbol{H}}{\partial t} , \tag{8.13}$$

$$\nabla \times \boldsymbol{H} = \boldsymbol{J}_\mathrm{i} + \sigma \boldsymbol{E} + \varepsilon \frac{\partial \boldsymbol{E}}{\partial t} , \tag{8.14}$$

$$\nabla \cdot \boldsymbol{E} = \frac{q_\mathrm{e}}{\varepsilon} , \tag{8.15}$$

$$\nabla \cdot \boldsymbol{H} = \frac{q_\mathrm{m}}{\mu} . \tag{8.16}$$

Taking the curl of both sides of (8.13) and (8.14) produces

$$\nabla \times \nabla \times \boldsymbol{E} = -\nabla \times \boldsymbol{M}_\mathrm{i} - \mu \frac{\partial}{\partial t} (\nabla \times \boldsymbol{H}) , \tag{8.17}$$

$$\nabla \times \nabla \times \boldsymbol{H} = \nabla \times \boldsymbol{J}_\mathrm{i} + \sigma \nabla \times \boldsymbol{E} + \varepsilon \frac{\partial}{\partial t} (\nabla \times \boldsymbol{E}) . \tag{8.18}$$

Substituting (8.14) into the right-hand side of (8.17), and using the vector identity $\nabla \times \nabla \times \boldsymbol{A} = \nabla \cdot (\nabla \cdot \boldsymbol{A}) - \nabla^2 \boldsymbol{A}$ on the left-hand side, gives

$$\nabla (\nabla \cdot \boldsymbol{E}) - \nabla^2 \boldsymbol{E} = -\nabla \times \boldsymbol{M}_\mathrm{i} - \mu \frac{\partial \boldsymbol{J}_\mathrm{i}}{\partial t} - \mu\sigma \frac{\partial \boldsymbol{E}}{\partial t} - \mu\varepsilon \frac{\partial^2 \boldsymbol{E}}{\partial t^2} . \tag{8.19}$$

Using (8.15), (8.19) can be rewritten as

$$\nabla^2 \boldsymbol{E} = \nabla \times \boldsymbol{M}_\mathrm{i} + \frac{1}{\varepsilon} \nabla q_\mathrm{e} + \mu \frac{\partial \boldsymbol{J}_\mathrm{i}}{\partial t} + \mu\sigma \frac{\partial \boldsymbol{E}}{\partial t} + \mu\varepsilon \frac{\partial^2 \boldsymbol{E}}{\partial t^2} . \tag{8.20}$$

This is an uncoupled second-order differential equation for $\boldsymbol{E}$.

The same process can be applied to obtain an uncoupled second-order differential equation for $\boldsymbol{H}$. Substituting (8.13) into the right-hand side of (8.18) and using the vector identity from the above on the left-hand side results in

$$\nabla (\nabla \cdot \boldsymbol{H}) - \nabla^2 \boldsymbol{H} = \nabla \times \boldsymbol{J}_\mathrm{i} - \sigma \boldsymbol{M}_\mathrm{i} - \varepsilon \frac{\partial \boldsymbol{M}_\mathrm{i}}{\partial t} - \mu\sigma \frac{\partial \boldsymbol{H}}{\partial t} - \mu\varepsilon \frac{\partial^2 H}{\partial t^2} . \tag{8.21}$$

Substituting (8.16) into (8.21) and reducing gives

$$\nabla^2 \boldsymbol{H} = -\nabla \times \boldsymbol{J}_\mathrm{i} + \sigma \boldsymbol{M}_\mathrm{i} + \frac{1}{\mu} \nabla q_\mathrm{m} + \varepsilon \frac{\partial \boldsymbol{M}_\mathrm{i}}{\partial t} + \mu\sigma \frac{\partial \boldsymbol{H}}{\partial t} + \mu\varepsilon \frac{\partial^2 \boldsymbol{H}}{\partial t^2} . \tag{8.22}$$

Equations (8.20) and (8.22) are vector wave equations for $\boldsymbol{E}$ and $\boldsymbol{H}$.

Only time-harmonic electromagnetic fields will be considered here. Time-harmonic fields can be represented by the real part of $\mathrm{e}^{\mathrm{i}\omega t}$, where ω is the angular frequency given by $2\pi f$, f is the linear frequency of the electromagnetic wave in hertz (Hz), and $i = \sqrt{-1}$. Since it is understood that $\mathrm{e}^{\mathrm{i}\omega t}$ appears in each term of Maxwell's equations, in can be dropped from the notation, allowing (8.5) through (8.8) to be rewritten as

$$\nabla \times \boldsymbol{E} = -\boldsymbol{M}_\mathrm{i} - \mathrm{i}\omega\mu \boldsymbol{H} , \tag{8.23}$$

$$\nabla \times \boldsymbol{H} = \boldsymbol{J}_\mathrm{i} + \boldsymbol{J}_\mathrm{c} + \mathrm{i}\omega\varepsilon \boldsymbol{E} , \tag{8.24}$$

$$\nabla \cdot \boldsymbol{E} = \frac{q_\mathrm{e}}{\varepsilon} , \tag{8.25}$$

$$\nabla \cdot \boldsymbol{H} = \frac{q_\mathrm{m}}{\mu} , \tag{8.26}$$

while the time-harmonic vector wave equations become

$$\nabla^2 \boldsymbol{E} = \nabla \times \boldsymbol{M}_\mathrm{i} + \frac{1}{\varepsilon}\nabla q_\mathrm{e} + \mathrm{i}\omega\mu \boldsymbol{J}_\mathrm{i} + \mathrm{i}\omega\mu\sigma \boldsymbol{E} - \omega^2 \mu\varepsilon \boldsymbol{E} \,, \tag{8.27}$$

$$\nabla^2 \boldsymbol{H} = -\nabla \times \boldsymbol{J}_\mathrm{i} + \sigma \boldsymbol{M}_\mathrm{i} + \frac{1}{\mu}\nabla q_\mathrm{m} + \mathrm{i}\omega\varepsilon \boldsymbol{M}_\mathrm{i} + \mathrm{i}\omega\mu\sigma \boldsymbol{H} - \omega^2 \mu\varepsilon \boldsymbol{H} \,. \tag{8.28}$$

Although $\boldsymbol{J}_\mathrm{i}$ and q_e can represent either real or virtual sources, $\boldsymbol{M}_\mathrm{i}$ and q_m are only virtual. In a source free region, $\boldsymbol{J}_\mathrm{i} = q_\mathrm{e} = 0$ and $\boldsymbol{M}_\mathrm{i} = q_\mathrm{m} = 0$, so that (8.27) and (8.28) reduce to the homogenous form of the wave equation

$$\nabla^2 \boldsymbol{E} - \gamma^2 \boldsymbol{E} = 0 \,, \tag{8.29}$$

$$\nabla^2 \boldsymbol{H} - \gamma^2 \boldsymbol{H} = 0 \,, \tag{8.30}$$

where

$$\gamma^2 = \mathrm{i}\omega\mu\sigma - \omega^2\mu\varepsilon \,. \tag{8.31}$$

Equations (8.29) and (8.30) describe electromagnetic waves traveling in a lossy medium with a propagation constant given by γ.

The last equations needed to completely define electromagnetic fields in the ocean are boundary conditions. Boundary conditions describe how the fields respond at an interface formed between two media of different constitutive properties, such as at the sea surface and seafloor. In this case, air is nonconducting with a permittivity and permeability the same as free space, while seawater is conductive with a high permittivity. Although the seafloor is conductive, its effective conductivity is one to four orders of magnitude less than the ocean's; depending on the depth the fields propagate below the bottom.

The generalized boundary conditions are well known. Their detailed derivation from Maxwell's equations can be found in [8.2]. Let the unit normal at the interface between two different media be given by $\hat{n}$ and pointing into the second region. Let the fields in media 1 and 2 be given by $\boldsymbol{E}_1$, $\boldsymbol{H}_1$, $\boldsymbol{D}_1$, $\boldsymbol{B}_1$ and $\boldsymbol{E}_2$, $\boldsymbol{H}_2$, $\boldsymbol{D}_2$, $\boldsymbol{B}_2$, respectively. Then the boundary conditions at the interface between them are

$$-\hat{n} \times (\boldsymbol{E}_2 - \boldsymbol{E}_1) = \boldsymbol{M}_\mathrm{s} \,, \tag{8.32}$$

$$\hat{n} \times (\boldsymbol{H}_2 - \boldsymbol{H}_1) = \boldsymbol{J}_\mathrm{s} \,, \tag{8.33}$$

$$\hat{n} \cdot (\boldsymbol{D}_2 - \boldsymbol{D}_1) = q_\mathrm{es} \,, \tag{8.34}$$

$$\hat{n} \cdot (\boldsymbol{B}_2 - \boldsymbol{B}_1) = q_\mathrm{ms} \,, \tag{8.35}$$

where $\boldsymbol{M}_\mathrm{s}$ and $\boldsymbol{J}_\mathrm{s}$ are the linear magnetic and electric surface currents along the boundary, and q_es and q_ms are the linear surface charge densities on the boundary. Although $\boldsymbol{M}_\mathrm{s}$ and q_ms are virtual boundary sources, they do arise in equivalent source representations of the fields within a closed region.

8.3 Plane Wave Propagation

The homogenous wave (8.29) and (8.30) can be solved in any of the separable coordinate systems. Their solution in rectangular coordinates will result in the expressions for plane waves. Using the method of separation of variables, the solution to (8.29) and (8.30) for a wave traveling along the positive z-axis is

$$\boldsymbol{E} = \boldsymbol{E}_0 \mathrm{e}^{-\gamma z} \,, \tag{8.36}$$

$$\boldsymbol{H} = \boldsymbol{H}_0 \mathrm{e}^{-\gamma z} \,, \tag{8.37}$$

where $\boldsymbol{E}_0$ and $\boldsymbol{H}_0$ are the amplitudes of the electric and magnetic fields. The propagation constant γ, defined by (8.31), can be written as

$$\gamma = \sqrt{\mathrm{i}\omega\mu(\sigma + \mathrm{i}\omega\varepsilon)} \,, \tag{8.38a}$$

$$\gamma = \alpha + \mathrm{i}\beta \,, \tag{8.38b}$$

and α is the attenuation constant in Np/m, and β is the phase constant in rad/m. If the waves were traveling in the negative z direction, then z in (8.36) and (8.37) would be replaced by $-z$. Solutions to the homogenous wave equation in cylindrical and spherical coordinates are derived in [8.2, pp. 12–18].

The electric and magnetic fields in (8.36) and (8.37) are linked through Maxwell's equations. For a source-free region, (8.24) can be written as

$$\boldsymbol{E} = \frac{1}{\sigma + \mathrm{i}\omega\varepsilon} \nabla \times \boldsymbol{H} \,. \tag{8.39}$$

If the magnetic field vector $\boldsymbol{H}$ in (8.39) has only an x component, given by H_x, taking its curl and substituting it in (8.36) gives

$$E_\mathrm{y} = \frac{-\gamma}{\sigma + \mathrm{i}\omega\varepsilon} H_\mathrm{x} \,. \tag{8.40}$$

Substituting (8.38a) into (8.40) and reducing gives

$$E_\mathrm{y} = -\eta H_\mathrm{x} \,, \tag{8.41}$$

where

$$\eta = \sqrt{\frac{\mathrm{i}\omega\mu}{\sigma + \mathrm{i}\omega\varepsilon}} \,. \tag{8.42}$$

The term η is called the *intrinsic impedance* of the medium and has the units of Ω. For a plane wave, the orthogonal electric and magnetic field components perpendicular to the propagation direction are related by the media's impedance.

In this section, only the ULF and ELF bands will be considered. Using the seawater dielectric permittivity constant from above, $\omega\varepsilon$ at the high end of the ELF band (3 kHz) is equal to $\approx 1.337\times10^{-5}$, which is much less than the water conductivity of 2.5 to 6. Therefore, the $\mathrm{i}\omega\varepsilon$ term will be dropped for electromagnetic frequencies up through the ELF band. In fact, displacement currents in seawater do not become appreciable until frequencies approach the high megahertz region.

At ELF frequencies and below, the seawater's attenuation constant is equal to its phase constant. Eliminating the $\mathrm{i}\omega\varepsilon$ in (8.38) gives

$$\gamma = \sqrt{\mathrm{i}\omega\mu\sigma}\,, \tag{8.43a}$$

$$\gamma = \sqrt{\frac{\omega\mu\sigma}{2}}(1+\mathrm{i})\,, \tag{8.43b}$$

$$\alpha = \beta = \sqrt{\frac{\omega\mu\sigma}{2}}\,. \tag{8.43c}$$

The distance at which the wave attenuates to e^{-1} is called the skin depth, and is denoted by the term δ. The skin depth is the reciprocal of the attenuation constant, $\delta = \frac{1}{\alpha}$, which for seawater is

$$\delta = \sqrt{\frac{2}{\omega\mu\sigma}}\,. \tag{8.44}$$

The field's wavelength λ is related to the propagation by $\lambda = \frac{2\pi}{\beta}$, and in this case can be written as

$$\lambda = 2\pi\sqrt{\frac{2}{\omega\mu\sigma}}\,, \tag{8.45}$$

while the speed of an electromagnetic wave v, is equal to $f\lambda$, and in seawater is given by

$$v = \sqrt{\frac{2\omega}{\mu\sigma}}\,. \tag{8.46}$$

Finally, the intrinsic impedance of seawater at ELF frequencies and below is expressed as

$$\eta = \sqrt{\frac{\mathrm{i}\omega\mu}{\sigma}}\,. \tag{8.47}$$

In the ocean, an electromagnetic wave's skin depth and wavelength is inversely proportional to the square root of its frequency, while its speed and intrinsic impedance is directly proportional to it.

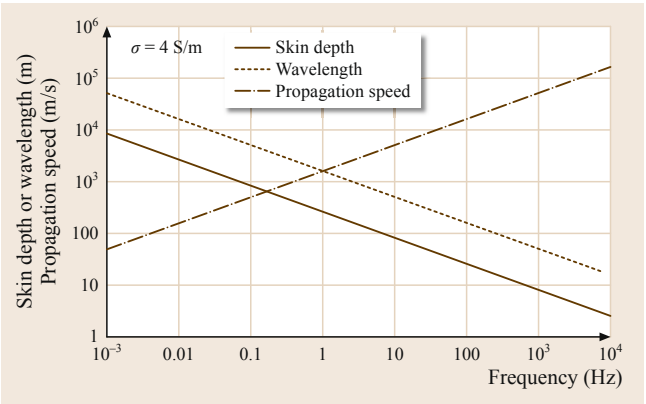

Fig. 8.1 Propagation characteristics of an electromagnetic wave in seawater

The characteristics of a propagating electromagnetic wave in the ocean are quite different than in air. In free space, the propagation speed of an electromagnetic field is always the same as that of light c (3×10^8 m/s), regardless of its frequency. This is not the case in the ocean. The skin depth, wavelength, and propagation speed given by (8.44) through (8.46) are plotted in Fig. 8.1 over the frequency range from 1 mHz to 10 kHz, using a seawater conductivity of 4 S/m. At 1 Hz, the skin depth is 252 m, while the wavelength and propagation speed are 1581 m and 1581 m/s. The propagation speed of electromagnetic fields in seawater at 1 Hz is more than 5 orders of magnitude slower than in air, and is approximately equal to the speed of sound in the ocean!

The intrinsic impedance of seawater is much smaller than free space. In air, η can be computed from (8.42) by setting $\sigma = 0$. This results in a free space impedance of 377 Ω, and is independent of frequency. Conversely, the intrinsic impedance of seawater

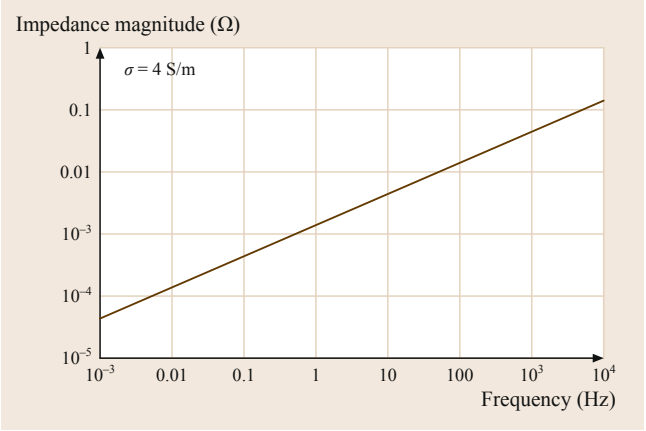

Fig. 8.2 Magnitude of the intrinsic impedance of seawater as a function of frequency

is $1.405\times10^{-3}(1+\mathrm{i})\,\Omega$ at 1 Hz. The magnitude of (8.47) has been plotted in Fig. 8.2 for the same parameters as above. As will be shown later, the difference in impedances between air and the ocean will significantly affect the reflection and transmission of electromagnetic fields at the sea surface.

As the frequency of the electromagnetic wave increases, so does its velocity. At the top end of the ELF band, an electromagnetic field propagates more than 100 times faster than sound, but the skin depth decreases to less than 3 m. For this reason, underwater electromagnetic communication systems for short distance wireless data transfers are preferred over acoustic modems. In addition, the rapid attenuation of electromagnetic fields in the ocean can be exploited to reduce interference from nearby transmitters, and for covert underwater communications systems that must avoid long range detection.

Another advantage of ULF and ELF electromagnetic fields is their ability to cross the air–ocean boundary. The description of plane wave transmission from air into conducting seawater is more complex than for fresh water. Therefore, the formulation of the *reflection and transmission coefficients* at the sea surface will begin with that of a plane wave incident on fresh water, such as a lake.

8.4 Reflection and Transmission of a Plane Wave at the Surface of Fresh Water

The reflection and transmission coefficients of a plane wave at the surface of fresh water depend on the polarization of the incident field. If the electric field vector of the incident uniform plane wave is perpendicular to the plane of incidence as shown in Fig. 8.3, then the wave is said to have a *perpendicular polarization* or *horizontal polarization*. Using the coordinate system and geometry of Fig. 8.3, the incident perpendicular polarized electric $\boldsymbol{E}^{\mathrm{i}}_{\perp}$ and magnetic $\boldsymbol{H}^{\mathrm{i}}_{\perp}$ field of a uniform plane wave can be written as

$$\boldsymbol{E}^{\mathrm{i}}_{\perp} = \hat{a}_{\mathrm{y}} E_0 \mathrm{e}^{-\mathrm{i}\beta_{\mathrm{a}}(x\sin\theta_{\mathrm{i}}+z\cos\theta_{\mathrm{i}})}\,, \tag{8.48}$$

$$\boldsymbol{H}^{\mathrm{i}}_{\perp} = (-\hat{a}_{\mathrm{x}}\cos\theta_{\mathrm{i}} + \hat{a}_{\mathrm{z}}\sin\theta_{\mathrm{i}}) \frac{E_0}{\eta_{\mathrm{a}}}\mathrm{e}^{-\mathrm{i}\beta_{\mathrm{a}}(x\sin\theta_{\mathrm{i}}+z\cos\theta_{\mathrm{i}})}\,, \tag{8.49}$$

where E_0 is the amplitude of the incident electric field, β_{a} is the propagation constant for the incident wave in air, η_{a} is the intrinsic impedance of air (377 Ω), θ_{i} is the incidence angle with respect to the vertical, and $\hat{a}_{\mathrm{x}}$, $\hat{a}_{\mathrm{y}}$, $\hat{a}_{\mathrm{z}}$ are the unit vectors in their respective directions. The relationship between the electric and magnetic field components for a uniform plane wave given by (8.41) was used to arrive at (8.49). Similarly, the reflected electric $\boldsymbol{E}^{\mathrm{r}}_{\perp}$ and magnetic $\boldsymbol{H}^{\mathrm{r}}_{\perp}$ plane waves are given by

$$\boldsymbol{E}^{\mathrm{r}}_{\perp} = \hat{a}_{\mathrm{y}}\Gamma_{\perp}E_0\mathrm{e}^{-\mathrm{i}\beta_{\mathrm{a}}(x\sin\theta_{\mathrm{r}}-z\cos\theta_{\mathrm{r}})}\,, \tag{8.50}$$

$$\boldsymbol{H}^{\mathrm{r}}_{\perp} = (\hat{a}_{\mathrm{x}}\cos\theta_{\mathrm{r}} + \hat{a}_{\mathrm{z}}\sin\theta_{\mathrm{r}}) \times \frac{\Gamma_{\perp}E_0}{\eta_{\mathrm{a}}}\mathrm{e}^{-\mathrm{i}\beta_{\mathrm{a}}(x\sin\theta_{\mathrm{r}}-z\cos\theta_{\mathrm{r}})}\,, \tag{8.51}$$

where $\Gamma_{\perp}$ is the reflection coefficient for a perpendicular polarized wave, and θ_{r} is the angle of the reflected wave with respect to the vertical. Finally, the transmitted electric $\boldsymbol{E}^{\mathrm{t}}_{\perp}$ and magnetic $\boldsymbol{H}^{\mathrm{t}}_{\perp}$ field can be expressed as

$$\boldsymbol{E}^{\mathrm{t}}_{\perp} = \hat{a}_{\mathrm{y}}T_{\perp}E_0\mathrm{e}^{-\mathrm{i}\beta_{\mathrm{f}}(x\sin\theta_{\mathrm{t}}+z\cos\theta_{\mathrm{t}})}\,, \tag{8.52}$$

$$\boldsymbol{H}^{\mathrm{t}}_{\perp} = (-\hat{a}_{\mathrm{x}}\cos\theta_{\mathrm{t}} + \hat{a}_{\mathrm{z}}\sin\theta_{\mathrm{t}}) \times \frac{T_{\perp}E_0}{\eta_{\mathrm{f}}}\mathrm{e}^{-\mathrm{i}\beta_{\mathrm{f}}(x\sin\theta_{\mathrm{t}}+z\cos\theta_{\mathrm{t}})}\,, \tag{8.53}$$

where $T_{\perp}$ is the transmission coefficient for a perpendicular polarized wave, and θ_{t} is the angle of the transmitted wave or *refraction angle* with respect to the vertical, and β_{f} and η_{f} are the propagation constant and intrinsic impedance of freshwater, respectively.

Equations (8.48)–(8.53) can be related through the boundary conditions of the continuity of the horizontal components of the electric and magnetic fields at the surface of the water. Since there are no sources at the air–water interface, $\boldsymbol{M}_{\mathrm{s}}$ and $\boldsymbol{J}_{\mathrm{s}}$ in (8.32) and (8.33)

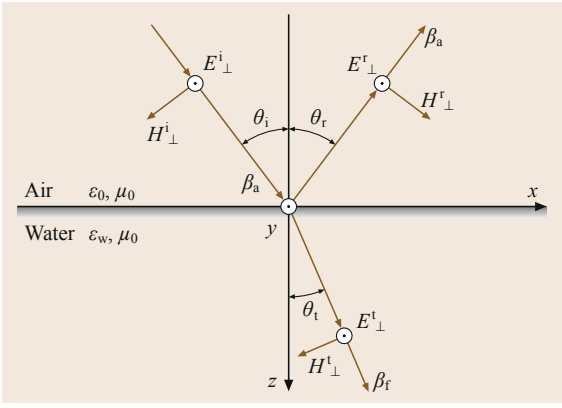

Fig. 8.3 Plane wave incident on the surface of fresh water, perpendicular polarization

are set to zero. Applying these boundary conditions to (8.48)–(8.53) at z = 0 gives

$$e^{-i\beta_a x \sin\theta_i} + \Gamma_\perp e^{-i\beta_a x \sin\theta_r} = T_\perp e^{-i\beta_f x \sin\theta_t} , \quad (8.54)$$

$$\frac{1}{\eta_a}\left(-\cos\theta_i e^{-i\beta_a x \sin\theta_i} + \cos\theta_r \Gamma_\perp e^{-i\beta_a x \sin\theta_r}\right) = -\frac{T_\perp}{\eta_f}\cos\theta_t e^{-i\beta_f x \sin\theta_t} . \quad (8.55)$$

Equations (8.54) and (8.55) are sufficient to solve for θ_r, θ_t, $\Gamma_\perp$, and $T_\perp$.

Breaking (8.54) and (8.55) into their real and imaginary parts will produce four equations with which to solve for the four unknowns. Following this procedure results in the relationships between the incident, reflected, and transmission angles given by

$$\theta_r = \theta_i , \quad (8.56a)$$

$$\beta_a \sin\theta_i = \beta_f \sin\theta_t . \quad (8.56b)$$

Equations (8.56a) and (8.56b) are called *Snell's laws* of reflection and refraction, respectively. Placing (8.56a) and (8.56b) into (8.54) and (8.55) and solving for the reflection and transmission coefficients produces the expressions

$$\Gamma_\perp = \frac{\boldsymbol{E}^r_\perp}{\boldsymbol{E}^i_\perp} = \frac{\eta_f \cos\theta_i - \eta_a \cos\theta_t}{\eta_f \cos\theta_i + \eta_a \cos\theta_t} , \quad (8.57)$$

$$T_\perp = \frac{\boldsymbol{E}^t_\perp}{\boldsymbol{E}^i_\perp} = \frac{2\eta_f \cos\theta_i}{\eta_f \cos\theta_i + \eta_a \cos\theta_t} . \quad (8.58)$$

Because air and water are both nonmagnetic (8.57) and (8.58) can be reduced to

$$\Gamma_\perp = \frac{\cos\theta_i - \sqrt{\varepsilon_w} cos\theta_t}{\cos\theta_i + \sqrt{\varepsilon_w}\cos\theta_t} , \quad (8.59)$$

$$T_\perp = \frac{2\cos\theta_i}{\cos\theta_i + \sqrt{\varepsilon_w}\cos\theta_t} , \quad (8.60)$$

where ε_w is the dielectric constant of water defined previously as 80.1.

A similar procedure is used to obtain the reflection and transmission coefficients for a uniform plane wave that has a *parallel polarization* incident on the surface of fresh water. A wave of this type also referred to as having a *vertical polarization* has an electric field that is parallel to the plane of incidence as shown in Fig. 8.4. Using the coordinate system and geometry of Fig. 8.4, the incident parallel polarized electric $\boldsymbol{E}^i_\parallel$ and magnetic $\boldsymbol{H}^i_\parallel$ field of a uniform plane wave can be written as

$$\boldsymbol{E}^i_\parallel = (\hat{a}_x \cos\theta_i - \hat{a}_z \sin\theta_i) E_0 e^{-i\beta_a(x\sin\theta_i + z\cos\theta_i)} , \quad (8.61)$$

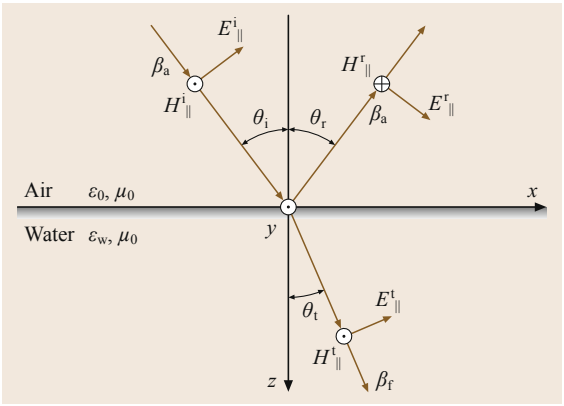

Fig. 8.4 Plane wave incident on the surface of fresh water, parallel polarization

$$\boldsymbol{H}^i_\parallel = \hat{a}_y \frac{E_0}{\eta_a} e^{-i\beta_a(x\sin\theta_i + z\cos\theta_i)} . \quad (8.62)$$

Similarly, the reflected electric $\boldsymbol{E}^r_\parallel$ and magnetic $\boldsymbol{H}^r_\parallel$ plane waves are given by

$$\boldsymbol{E}^r_\parallel = (\hat{a}_x \cos\theta_r + \hat{a}_z \sin\theta_r)\Gamma_\parallel E_0 e^{-i\beta_a(x\sin\theta_r - z\cos\theta_r)} , \quad (8.63)$$

$$\boldsymbol{H}^r_\parallel = -\hat{a}_y \frac{\Gamma_\parallel E_0}{\eta_a} e^{-i\beta_a(x\sin\theta_r - z\cos\theta_r)} , \quad (8.64)$$

and the transmitted electric $\boldsymbol{E}^t_\parallel$ and magnetic $\boldsymbol{H}^t_\parallel$ plane waves are

$$\boldsymbol{E}^t_\parallel = (\hat{a}_x \cos\theta_t - \hat{a}_z \sin\theta_t) T_\parallel E_0 e^{-i\beta_f(x\sin\theta_t + z\cos\theta_t)} , \quad (8.65)$$

$$\boldsymbol{H}^t_\parallel = \hat{a}_y \frac{T_\parallel E_0}{\eta_f} e^{-i\beta_f(x\sin\theta_t + z\cos\theta_t)} , \quad (8.66)$$

where $\Gamma_\parallel$ and $T_\parallel$ represent the reflection and transmission coefficients for a parallel polarized incident wave, respectively. All other parameters have been defined previously.

The analysis proceeds in the same manner as used for the perpendicular polarized waves. Applying the continuity boundary conditions for the tangential components of the electric and magnetic fields at the air–water interface ($z = 0$) give the equations

$$\cos\theta_i e^{-i\beta_a x \sin\theta_i} + \cos\theta_r \Gamma_\parallel e^{-i\beta_a x \sin\theta_r} = \cos\theta_t T_\parallel e^{-i\beta_f x \sin\theta_t} , \quad (8.67)$$

$$\frac{1}{\eta_a}\left(e^{-i\beta_a x \sin\theta_i} - \Gamma_\parallel e^{-i\beta_a x \sin\theta_r}\right) = \frac{T_\parallel}{\eta_f} e^{-i\beta_f x \sin\theta_t} . \quad (8.68)$$

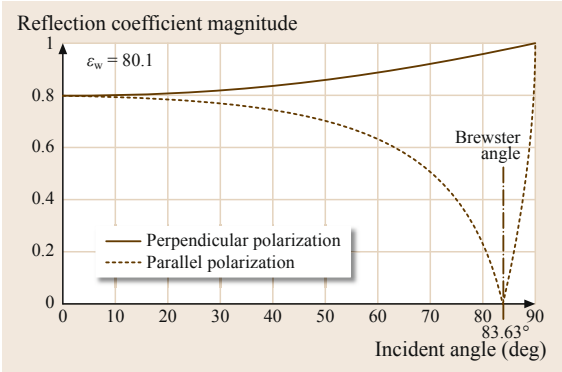

Fig. 8.5 Reflection coefficients for a perpendicular and parallel polarized uniform plane wave incident on the surface of fresh water

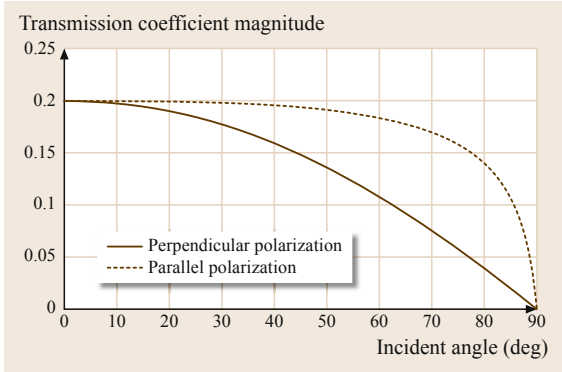

Fig. 8.6 Transmission coefficients for a perpendicular and parallel polarized uniform plane wave incident on the surface of fresh water

Once again, equating the real and imaginary parts of (8.67) and (8.68) will yield Snell's laws of reflection and refraction (8.56a) and (8.56b), along with the reflection and transmission coefficients for parallel polarization written as

$$\Gamma_{\parallel} = \frac{\boldsymbol{E}^{\mathrm{r}}_{\parallel}}{\boldsymbol{E}^{\mathrm{i}}_{\parallel}} = \frac{-\eta_{\mathrm{a}} \cos\theta_{\mathrm{i}} + \eta_{\mathrm{f}} \cos\theta_{\mathrm{t}}}{\eta_{\mathrm{a}} \cos\theta_{\mathrm{i}} + \eta_{\mathrm{f}} \cos\theta_{\mathrm{t}}} , \tag{8.69}$$

$$T_{\parallel} = \frac{\boldsymbol{E}^{\mathrm{t}}_{\parallel}}{\boldsymbol{E}^{\mathrm{i}}_{\parallel}} = \frac{2\eta_{\mathrm{f}} \cos\theta_{\mathrm{i}}}{\eta_{\mathrm{a}} \cos\theta_{\mathrm{i}} + \eta_{\mathrm{f}} \cos\theta_{\mathrm{t}}} . \tag{8.70}$$

For the interface between air and fresh water, (8.69) and (8.70) reduce to

$$\Gamma_{\parallel} = \frac{-\sqrt{\epsilon}_{\mathrm{w}} \cos\theta_{\mathrm{i}} + \cos\theta_{\mathrm{t}}}{\sqrt{\epsilon}_{\mathrm{w}} \cos\theta_{\mathrm{i}} + \cos\theta_{\mathrm{t}}} , \tag{8.71}$$

$$T_{\parallel} = \frac{2\cos\theta_{\mathrm{i}}}{\sqrt{\epsilon}_{\mathrm{w}} \cos\theta_{\mathrm{i}} + \cos\theta_{\mathrm{t}}} . \tag{8.72}$$

Although (8.59) and (8.60) are similar in form to (8.71) and (8.72), a simple example will highlight the differences.

The reflection and transmission coefficients for perpendicular and parallel polarizations were evaluated for a plane wave incident on the surface of fresh water with a dielectric constant of 80.1. Using Snell's law of refraction (8.56) at the air–water interface, the $\cos\theta_{\mathrm{t}}$ term in (8.59), (8.60), (8.71), and (8.72) can be computed from

$$\cos\theta_{\mathrm{t}} = \sqrt{1 - \frac{1}{\varepsilon_{\mathrm{w}}} \sin^2\theta_{\mathrm{i}}} . \tag{8.73}$$

The magnitudes of $\Gamma_{\perp}$ and $\Gamma_{\parallel}$ are plotted in Fig. 8.5 for all incidence angles from 0 to 90°, while $T_{\perp}$, and $T_{\parallel}$ are similarly plotted in Fig. 8.6. Interestingly, $\Gamma_{\parallel}$ goes through zero at an angle of 83.63°. This angle is called the *Brewster angle* for which there is no reflection from the water's surface. The Brewster angle only exists for incident plane waves that have parallel polarization.

8.5 Plane Wave Incident on Seawater

The general forms of the reflection and transmission coefficients computed for fresh water are also valid when the wave is incident on the surface of the electrically conducting ocean. In this case, the intrinsic impedance of fresh water η_{f} used in (8.57), (8.58), (8.69), and (8.70) is replaced with that of seawater η_{s} given by (8.47). Since η_{s} is a complex impedance with both real and imaginary parts, $\Gamma_{\perp}$, $T_{\perp}$, $\Gamma_{\parallel}$, and $T_{\parallel}$ will all be complex. This means that both the amplitude and phase of the reflected and transmitted fields will be modified by the ocean's surface.

The most dramatic effect of the sea surface on a uniform plane wave is its impact on the transmitted field's propagation characteristics. Rewriting Snell's law of refraction (8.56b) for seawater gives

$$\mathrm{i}\beta_{\mathrm{a}} \sin\theta_{\mathrm{i}} = \gamma \sin\theta_{\mathrm{t}} , \tag{8.74}$$

where γ has both a real and imaginary part given by (8.43c). In this case, the $\sin\theta_{\mathrm{t}}$ term in (8.74) can be expressed as

$$\sin\theta_{\mathrm{t}} = \frac{\mathrm{i}\beta_{\mathrm{a}}}{\alpha + \mathrm{i}\beta} \sin\theta_{\mathrm{i}} . \tag{8.75}$$

Using (8.75) and the identity $\cos\theta_t = \sqrt{1-\sin^2\theta_t}$, the term $\cos\theta_t$ becomes

$$\cos\theta_t = \sqrt{1-\left(\frac{i\beta_a}{\alpha+i\beta}\right)^2 \sin^2\theta_i}\,, \tag{8.76}$$

which can be reduced to a general form of

$$\cos\theta_t = s e^{i\xi}\,. \tag{8.77}$$

It is clear that the wave transmitted into the sea will be at an angle that is complex. The idea of a real and imaginary transmission angle needs further explanation.

The electric field for a perpendicular or parallel polarized field transmitted into seawater, (8.52) or (8.65), can be written in a general form given by

$$\boldsymbol{E}^t = \boldsymbol{E}_0^t e^{-\gamma(x\sin\theta_t + z\cos\theta_t)}\,, \tag{8.78}$$

that can be expanded to

$$\boldsymbol{E}^t = \boldsymbol{E}_0^t \exp[-(\alpha+i\beta)(x\sin\theta_t + z\cos\theta_t)]\,. \tag{8.79}$$

All the terms in front of the exponential in either (8.52) or (8.65) have been lumped into $\boldsymbol{E}_0^t$. Placing (8.75) and (8.77) into (8.79) gives

$$\boldsymbol{E}^t = \boldsymbol{E}_0^t \exp\left[-(\alpha+i\beta)\left(x\frac{i\beta_a}{\alpha+i\beta}\sin\theta_i + zs(\cos\xi + i\sin\xi)\right)\right], \tag{8.80}$$

and can be reduced to

$$\boldsymbol{E}^t = \boldsymbol{E}_0^t e^{-zp}\exp[-i(x\beta_a\sin\theta_i + zq)]\,, \tag{8.81}$$

where

$$p = s(\alpha\cos\xi - \beta\sin\xi)\,, \tag{8.82}$$

$$q = s(\alpha\sin\xi + \beta\cos\xi)\,. \tag{8.83}$$

The expression given by (8.81) describes a nonuniform wave.

A plane wave refracted into conducting seawater has planes of constant amplitude and phase that are not coincident. Equation (8.81) shows that the planes of constant amplitude (z = constant) are parallel to the ocean's surface as drawn in Fig. 8.7. The attenuation vector of the refracted wave is $\hat{\alpha}_s = \hat{a}_z p$, where p is the attenuation constant. To find the direction of propagation of the refracted wave, the phase term given in (8.81) is rewritten as

$$x\beta_a\sin\theta_i + zq = \beta_s(x\sin\Psi + z\cos\Psi)\,, \tag{8.84}$$

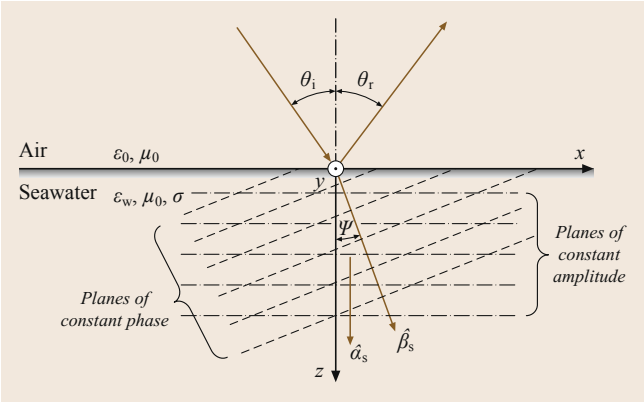

Fig. 8.7 Plane wave refracted into seawater

where

$$\beta_s = \sqrt{u^2+q^2}\,, \tag{8.85}$$

$$\sin\Psi = \frac{u}{\sqrt{u^2+q^2}}\,, \tag{8.86}$$

$$\cos\Psi = \frac{q}{\sqrt{u^2+q^2}}\,, \tag{8.87}$$

$$u = \beta_a\sin\theta_i\,. \tag{8.88}$$

The phase propagation direction for the refracted wave is $\hat{\beta}_s = \hat{a}_x\sin\Psi + \hat{a}_z\cos\Psi$, and produces planes of constant phase perpendicular to $\hat{\beta}_s$ as drawn in Fig. 8.7. The angle of refraction for the direction of propagation is determined from

$$\Psi = \tan^{-1}\left(\frac{u}{q}\right). \tag{8.89}$$

The phase velocity of the refracted wave is given by

$$v_r = \frac{\omega}{\beta_s}\,. \tag{8.90}$$

The refracted wave's attenuation, direction of propagation and velocity are all dependent on the incident angle; but to what extent? Another example is in order.

In this example, a 1 Hz plane wave is incident on the surface of the open ocean at an oblique angle θ_i. Using the intrinsic parameters for air $\sigma = 0$, μ_0, and ε_0 in (8.38) and (8.42), the free space propagation constant β_a is equal to $\frac{\omega}{c}$ (c is the speed of light in a vacuum is 3×10^8 m/s), and the intrinsic impedance of air is 377 Ω that is independent of frequency. For a seawater conductivity of 4 S/m, (8.76) can be written as

$$\cos\theta_t \approx \sqrt{1-(-i2.2\times10^{-11})\sin^2\theta_i} \approx 1$$

for all angles of incidence. This produces the values $s = 1$, $\xi = 0$, and $q = \beta$ from (8.77) and (8.83). The electromagnetic wave's angle of refraction in the ocean, given by (8.89), reduces to

$$\Psi = \tan^{-1}\left(\frac{\omega}{c\beta}\sin\theta_\mathrm{i}\right). \tag{8.91}$$

At 1 Hz, $\frac{\omega}{c\beta} = 5.27\times10^{-6}$, and the maximum angle of refraction is $\Psi_{\max} \le \tan^{-1}(5.27\times10^{-6})$ or $\Psi_{\max} \le 3\times10^{-4\circ}$ (≈ 1 s of an arc). Even at 3 kHz the refracted angle is computed to be less than 0.02°. Therefore, for frequencies up through the ELF band, a plane wave incident on the surface of the ocean at any angle will refract, propagate, and attenuate toward the bottom along a path that is nearly vertical.

The analysis presented above for a single interface can be extended to include any number of layers with different intrinsic parameters. The derivation of the iterative equation can be found in [8.2, pp. 110–120]. Plane wave reflection and transmission for multilayered ocean environments would arise when modeling depth variations of uniformly stratified seawater or seafloor conductivities.

8.6 Magnetic and Electric Dipoles in an Unbounded Ocean

Strictly speaking, plane waves do not exist in nature. They can be used to approximate an electromagnetic field that is far from its source (transmitter), or in the case where a uniform distribution of sources extend to very large distances in comparison to the receiver's range to it. An example of the latter case would be the geomagnetic fields present at the ocean's surface generated by solar-wind-induced electric currents in the ionosphere.

The two elemental sources of electromagnetic fields are the electric and magnetic point dipoles. An electric dipole source p is created by an electric current I flowing in a conductor over a linear distance l ($p = Il$), and has units of A m. A magnetic dipole m is produced if the current flows around a closed circular path that encloses an area a ($m = Ia$), and has units of A m^2. If the observation point is at a distance that is large compared to the source's dimensions, then it can be represented mathematically as an infinitesimally small or point dipole. With sources present, the time-harmonic vector wave equations, (8.27) and (8.28), are now inhomogeneous.

Although it is possible to solve for the electric and magnetic fields directly from the inhomogeneous vector wave equations, it is generally mathematically advantageous to replace them with equivalent representations in terms of the *magnetic vector potential* $\boldsymbol{A}$ and *electric vector potential* $\boldsymbol{F}$. The solutions to the inhomogeneous vector wave equations in terms of vector potentials are derived in [8.3], and can be written as

$$\boldsymbol{E} = -\mathrm{i}\omega\boldsymbol{A} + \frac{1}{\mu\sigma}\nabla(\nabla\cdot\boldsymbol{A}) - \frac{1}{\varepsilon}\nabla\times\boldsymbol{F}\,, \tag{8.92}$$

$$\boldsymbol{H} = -\mathrm{i}\omega\boldsymbol{F} + \frac{1}{\mu\sigma}\nabla(\nabla\cdot\boldsymbol{F}) + \frac{1}{\mu}\nabla\times\boldsymbol{A}\,, \tag{8.93}$$

where

$$\boldsymbol{A} = \frac{\mu}{4\pi}\iiint_V \boldsymbol{J}_\mathrm{i}\frac{\mathrm{e}^{-\gamma R}}{R}\,\mathrm{d}v'\,, \tag{8.94}$$

$$\boldsymbol{F} = \frac{\varepsilon}{4\pi}\iiint_V \boldsymbol{M}_\mathrm{i}\frac{\mathrm{e}^{-\gamma R}}{R}\,\mathrm{d}v'\,, \tag{8.95}$$

$$R = \sqrt{(x-x')^2 + (y-y')^2 + (z-z')^2}\,, \tag{8.96}$$

and the elements of the impressed electric $\boldsymbol{J}_\mathrm{i}$ and magnetic $\boldsymbol{M}_\mathrm{i}$ current densities are located at (x', y', z') with the observation point at (x, y, z). The integration is taken over the entire volume of the source.

Equations (8.92)–(8.96) are sufficient to compute the electric and magnetic fields from dipole sources. Consider first an electric point dipole of strength p located at the origin of the coordinate system shown in Fig. 8.8, and aligned along the z-axis. The impressed source's electric current density for this dipole can be represented mathematically as

$$\boldsymbol{J}_\mathrm{i} = \hat{a}_z p\delta(x')\delta(y')\delta(z')\,, \tag{8.97}$$

where the δ used here represents the Dirac delta function. Placing (8.97) into (8.94) yields the magnetic vector potential

$$A_\mathrm{z} = \frac{\mu p\mathrm{e}^{-\gamma r}}{4\pi r}\,, \tag{8.98}$$

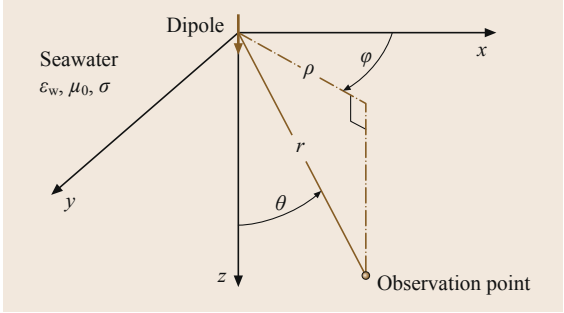

Fig. 8.8 Coordinate system for a dipole in an unbounded ocean

where r is the radial distance from the origin as shown in Fig. 8.8. Converting (8.98) to spherical coordinates and placing it into (8.92) and (8.93), the electric and magnetic fields of a point electric dipole in an unbounded ocean are written as

$$E_r = \frac{p\cos\theta}{2\pi\sigma r^3}(1+\gamma r)e^{-\gamma r}\,, \tag{8.99}$$

$$E_\theta = \frac{p\sin\theta}{4\pi\sigma r^3}(1+\gamma r+\gamma^2 r^2)e^{-\gamma r}\,, \tag{8.100}$$

$$H_\varphi = \frac{p\sin\theta}{4\pi r^2}(1+\gamma r)e^{-\gamma r}\,. \tag{8.101}$$

If the point dipole was located at coordinates (x_0, y_0, z_0) instead of the origin, then r becomes

$$\sqrt{(x-x_0)^2+(y-y_0)^2+(z-z_0)^2}\,.$$

The derivation of a magnetic point dipole follows that shown above for the electric. In this case, the magnetic point dipole has a source strength m that is also located at the origin, and is aligned along the z-axis. A dipole of this type could be produced by an electric current flowing in the φ direction of the coordinate system in Fig. 8.8. This is mathematically equivalent to a virtual magnetic current source aligned along the z-axis. Therefore, the equivalent impressed magnetic current density for this dipole can be written as

$$\boldsymbol{M}_i = \hat{a}_z m\delta(x')\delta(y')\delta(z')\,. \tag{8.102}$$

Using (8.102) in (8.95) yields the electric vector potential

$$F_z = \frac{\varepsilon m e^{-\gamma r}}{4\pi r}\,. \tag{8.103}$$

Converting (8.103) to spherical coordinates and placing it into (8.92) and (8.93), the electric and magnetic fields of a point magnetic dipole in an unbounded ocean can be written as

$$H_r = \frac{m\cos\theta}{2\pi r^3}(1+\gamma r)e^{-\gamma r}\,, \tag{8.104}$$

$$H_\theta = \frac{m\sin\theta}{4\pi r^3}(1+\gamma r+\gamma^2 r^2)e^{-\gamma r}\,, \tag{8.105}$$

$$E_\varphi = \frac{-i\omega\mu m\sin\theta}{4\pi r^2}(1+\gamma r)e^{-\gamma r}\,. \tag{8.106}$$

It should be noted that the electromagnetic fields for both the electric and magnetic dipole sources are circularly symmetric and are not a function of the φ coordinate.

The equations for the electromagnetic fields of electric and magnetic point dipoles in an unbounded ocean reduce to the standard static magnetic and electric expressions by setting the frequency in (8.99) to (8.101) and (8.104) to (8.106) to zero. Carrying this out gives the electric and magnetic fields of a static electric dipole in an unbounded ocean as

$$E_r = \frac{p\cos\theta}{2\pi\sigma r^3}\,, \tag{8.107}$$

$$E_\theta = \frac{p\sin\theta}{4\pi\sigma r^3}\,, \tag{8.108}$$

$$H_\varphi = \frac{p\sin\theta}{4\pi r^2}\,, \tag{8.109}$$

and for the static magnetic dipole (8.104) to (8.106) reduce to

$$H_r = \frac{m\cos\theta}{2\pi r^3}\,, \tag{8.110}$$

$$H_\theta = \frac{m\sin\theta}{4\pi r^3}\,, \tag{8.111}$$

$$E_\varphi = 0\,. \tag{8.112}$$

It should be noted that all electric and magnetic field components for static dipoles fall off in the radial direction as r^{-3} except for the φ component of the magnetic field of the static electric dipole, which fall off as r^{-2}, and the φ component of the electric field of the static magnetic dipole, which is zero.

Except for the zero E_φ component of the static magnetic dipole, the static and time-harmonic dipole equations differ by a factor of either $(1+\gamma r)e^{-\gamma r}$ or $(1+\gamma r+\gamma^2 r^2)e^{-\gamma r}$. The magnitude of these two multiplication factors are plotted in Fig. 8.9 as a function of the radial distance in skin depths. This data shows the range over which the electric and magnetic field equations for static sources can be used to estimate the time-harmonic fields. Depending on accuracy requirements, the static equations could be used out to distances approaching a skin depth. It is interesting that $|(1+\gamma r+\gamma^2 r^2)e^{-\gamma r}|$ is 1 at a distance equal to a half-

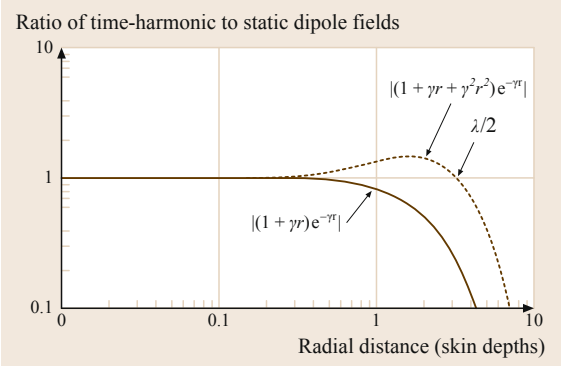

Fig. 8.9 Correction factors to convert electric and magnetic fields computed for static dipoles to those of time-harmonic sources

wavelength, as indicated in Fig. 8.9. The region in close vicinity to a time-harmonic dipole for which the static equations are sufficiently accurate is sometimes called the *quasi-DC* (direct current) range.

The equations for electric and magnetic dipoles in an unbounded ocean are sufficient if the range between the source and observation point is small in comparison to their distances from the sea surface or seafloor. If this is not the case, then reflections from one or both of the interfaces must be accounted for in the magnetic and electric field formulations. Since the dipole sources are close to an interface, simple plane wave reflection coefficients cannot be used. A more complete and, unfortunately, more complex treatment are required.

8.7 Magnetic and Electric Dipoles in a Bounded Ocean

In this section, magnetic and electric dipoles submerged in a bounded ocean will be considered. What is meant by *a bounded ocean* is that the separation between the source and observation point are comparable to their distance from either the sea surface or bottom. The change in conductivity between the seawater and air or the seafloor produces an interface that modifies the spreading and propagation of fields generated by submerged magnetic and electric sources. The effects of the interfaces are accounted for in the descriptive equations by satisfying the boundary conditions along them. Therefore, mathematical solutions to the inhomogeneous wave equations must be in a form that will easily accommodate solving for the boundary conditions when a source is near an interface.

Because of their close proximity to one of the ocean's interface, the solution to the problem of a submerged magnetic or electric dipole will also depend on their orientation with respect to the sea surface or seafloor. As a result, there are four types of dipoles that must be addressed separately when computing their electric and magnetic fields in a bounded ocean. They are; the vertical electric dipole (VED), vertical magnetic dipole (VMD), horizontal magnetic dipole (HMD), and the horizontal electric dipole (HED). The equations for the in-water fields from a subsurface time-harmonic VED in a deep ocean (only the surface interface) will be derived to demonstrate the analysis method. References will then be cited where solutions to the other source types can be found.

The geometry for a submerged vertical dipole and observation point is drawn in Fig. 8.10. As before, the air is nonconducting with free-space permittivity and permeability, while the ocean has its standard intrinsic parameters. The dipole is located on the z-axis at a depth h, with the observation point also located in the seawater at (ρ, φ, z). Although this problem can be solved in rectangular coordinates, cylindrical coordinates are employed due to the electromagnetic fields' circular symmetry about the source.

A slightly different form of the vector potential is typically used when solving the problem of dipoles in a layered medium. The alternate form is called the *Hertz* vector potential. For a VED, the electric Hertz vector potential, denoted by $\boldsymbol{\Pi}$, has only a z component and is given by

$$\Pi_z = \frac{p}{4\pi(\sigma + i\omega\epsilon)} \frac{e^{-\gamma r}}{r} , \tag{8.113}$$

where

$$r = \sqrt{\rho^2 + (z-h)^2} .$$

The general relationships between the magnetic vector potential, the electric *Hertz* vector potential, and the electric and magnetic fields are

$$\boldsymbol{A} = \mu(\sigma + i\omega\epsilon)\boldsymbol{\Pi} , \tag{8.114}$$

$$\boldsymbol{E} = -\gamma^2 \boldsymbol{\Pi} + \nabla(\nabla \cdot \boldsymbol{\Pi}) , \tag{8.115}$$

$$\boldsymbol{H} = -(\sigma + i\omega\epsilon)\nabla \times \boldsymbol{\Pi} . \tag{8.116}$$

Placing (8.113) in (8.115) and (8.116), and reducing them in cylindrical coordinates, gives

$$E_\rho = \frac{\partial^2 \Pi_z}{\partial \rho \partial z} , \tag{8.117}$$

$$E_z = -\gamma^2 \Pi_z + \frac{\partial^2 \Pi_z}{\partial z^2} , \tag{8.118}$$

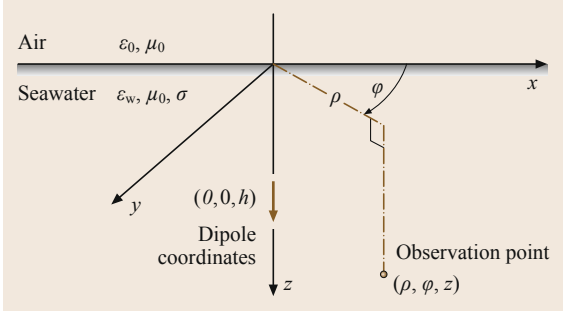

Fig. 8.10 Coordinate system for a submerged vertical dipole and submerged observation point in an electrically deep ocean

$$H_\varphi = -(\sigma + \mathrm{i}\omega\epsilon)\frac{\partial \Pi_z}{\partial \rho}\,, \tag{8.119}$$

and all other electric and magnetic field components are zero. Equations (8.113) through (8.119) apply to both the seawater and air using the appropriate constitutive parameters for each media.

The Hertz electric vector must be put in a form suitable for matching the boundary conditions at the surface interface. Using the identity

$$\frac{\mathrm{e}^{-\gamma r}}{4\pi r} = \frac{1}{4\pi}\int_0^\infty \frac{\lambda}{u}\mathrm{e}^{-u|z|}J_0(\lambda\rho)\,\mathrm{d}\lambda\,, \tag{8.120}$$

where J_0 is the Bessel function of order 0, and

$$u = (\lambda^2 + \gamma^2)^{\frac{1}{2}}\,, \tag{8.121}$$

the electric Hertz vector for a VED located at a depth h on the z-axis, (8.113), can be written as

$$\Pi_z^{(\mathrm{w})} = \frac{p}{4\pi(\sigma + \mathrm{i}\omega\varepsilon_\mathrm{w})}\int_0^\infty \frac{\lambda}{u_\mathrm{w}}\mathrm{e}^{-u_\mathrm{w}|z-h|}J_0(\lambda\rho)\,\mathrm{d}\lambda\,, \tag{8.122}$$

and the subscript and superscript, w, indicates that the constitutive parameters for seawater are to be applied. The integral representation in (8.122) can be replaced with

$$\int_0^\infty \frac{\lambda}{u_\mathrm{w}}\mathrm{e}^{-u_\mathrm{w}(z-h)}J_0(\lambda\rho)\,\mathrm{d}\lambda \quad \text{when } (z-h)\geq 0\,, \tag{8.123}$$

$$\int_0^\infty \frac{\lambda}{u_\mathrm{w}}\mathrm{e}^{u_\mathrm{w}(z-h)}J_0(\lambda\rho)\,\mathrm{d}\lambda \quad \text{when } (z-h)\leq 0\,. \tag{8.124}$$

Equations (8.120) and (8.122) are called *Hankel transforms* or *Sommerfeld integrals*.

Equation (8.122) must be modified to account for reflections from the surface interface, and an additional equation is needed to describe the transmitted fields in the air. The system of Hertz equations sufficient to solve for the electromagnetic fields in both the air $\Pi_z^{(\mathrm{a})}$ and seawater $\Pi_z^{(\mathrm{w})}$ layers are

$$\Pi_z^{(\mathrm{a})} = P_\mathrm{w}\int_0^\infty f_1(\lambda)\mathrm{e}^{u_0 z}J_0(\lambda\rho)\,\mathrm{d}\lambda \quad \text{for } z\leq 0\,, \tag{8.125}$$

$$\Pi_z^{(\mathrm{w})} = P_\mathrm{w}\int_0^\infty \frac{\lambda}{u_\mathrm{w}}\mathrm{e}^{-u_\mathrm{w}|z-h|}J_0(\lambda\rho)\,\mathrm{d}\lambda + P_\mathrm{w}\int_0^\infty f_2(\lambda)\mathrm{e}^{-u_\mathrm{w}z}J_0(\lambda\rho)\,\mathrm{d}\lambda \quad \text{for } z\geq 0\,, \tag{8.126}$$

where

$$P_\mathrm{w} = \frac{p}{4\pi\sigma}\,, \tag{8.127}$$

$$u_\mathrm{w} = (\lambda^2 + \gamma^2)^{\frac{1}{2}}\,, \tag{8.128}$$

$$u_0 = (\lambda^2 + \gamma_0^2)^{\frac{1}{2}}\,, \tag{8.129}$$

and $\gamma_0^2 = -\omega^2\mu_0\varepsilon_0$, while $\gamma^2 = \mathrm{i}\omega\mu_0\sigma$. The terms f_1 and f_2 are determined by the boundary conditions at the ocean surface.

The boundary conditions require that the tangential components of the electric and magnetic fields must be continuous across the sea surface. For this problem, E_ρ (8.117) and H_φ (8.119) are the components tangential to the interface. The continuation of these tangential field components can be expressed in terms of their electric Hertz vectors as

$$\left.\begin{aligned}\frac{\partial \Pi_z^{(\mathrm{a})}}{\partial z} &= \frac{\partial \Pi_z^{(\mathrm{w})}}{\partial z}\\ \gamma_0^2\Pi_z^{(\mathrm{a})} &= \gamma_\mathrm{w}^2\Pi_z^{(\mathrm{w})}\end{aligned}\right] \quad \text{at } z = 0\,. \tag{8.130}$$

Applying these boundary conditions results in a system of equations for f_1 and f_2 given by

$$\frac{u_0}{u_\mathrm{w}}f_1 + f_2 = \frac{\lambda}{u_\mathrm{w}}\mathrm{e}^{-u_\mathrm{w}h}\,, \tag{8.131}$$

$$\frac{\gamma_0^2}{\gamma_\mathrm{w}^2}f_1 - f_2 = \frac{\lambda}{u_\mathrm{w}}\mathrm{e}^{-u_\mathrm{w}h}\,. \tag{8.132}$$

Solving for f_1 and f_2 produces

$$f_1(\lambda) = \frac{\frac{2\lambda}{u_\mathrm{w}}\mathrm{e}^{-u_\mathrm{w}h}}{\frac{u_0}{u_\mathrm{w}} + \frac{\gamma_0^2}{\gamma_\mathrm{w}^2}}\,, \tag{8.133}$$

$$f_2(\lambda) = \frac{\lambda}{u_\mathrm{w}}\mathrm{e}^{-u_\mathrm{w}h}\left(-\frac{\frac{2u_0}{u_\mathrm{w}}}{\frac{u_0}{u_\mathrm{w}} + \frac{\gamma_0^2}{\gamma_\mathrm{w}^2}}\right). \tag{8.134}$$

Since $\gamma_0^2 \ll \gamma_\mathrm{w}^2$ for all frequencies up through the ELF band, γ_0 can be set to zero in (8.125), (8.133), and (8.134). Under these conditions, f_1 and f_2 reduce to

$$f_1(\lambda) = 2\mathrm{e}^{-u_\mathrm{w}h}\,, \tag{8.135}$$

$$f_2(\lambda) = -\frac{\lambda}{u_\mathrm{w}}\mathrm{e}^{-u_\mathrm{w}h}\,. \tag{8.136}$$

This *no-propagation* approximation for air is sometimes called the *quasi-static condition*, and should not be confused with the quasi-DC case discussed previously.

With the solutions to f_1 and f_2 in hand, (8.125) and (8.126) can be placed in (8.120) through (8.122) to compute the electric and magnetic fields above and below the sea surface. For some special cases, the field equations can be solved in the analytical form; but in general, the Sommerfeld integrals must be evaluated numerically. Unfortunately, the integrands are oscillatory and slowly damped, increasing the difficulty in their numerical integration. Special techniques have been developed to efficiently evaluate Sommerfeld-type integrals, most of which have been reviewed in [8.4].

Derivation of the more complicated equations for a VED in a shallow ocean, which includes the interface at the seafloor, follows the same procedure as shown above for the deep water analysis. In the shallow water case, a third Hertz vector is needed to describe propagation within the sea bottom, and another term must be included in (8.126) to account for reflections off the seafloor. Satisfying the boundary conditions at both the seafloor and sea surface produce four equations with four unknowns, this time f_1 through f_4. The Sommerfeld integral formulations for a VED in a three layer media can be found in [8.5], and applied to the shallow-ocean problem using the appropriate constitutive parameters.

The complementarity problem of a VMD in a deep or shallow ocean is solved in an analogous manner using a magnetic Hertz vector in place of the electric vector. The in-air fields from a time-harmonic VMD submerged in shallow water have been reported in [8.6], while the in-water fields from an airborne VMD are found in [8.7]. Because of the presence of the ocean surface and/or bottom interface, the field solutions for an HED require both horizontal and vertical electric Hertz vectors to satisfy the boundary conditions [8.8]. Although this complicates the algebra by doubling the number of boundary equations and unknowns, the Sommerfeld formulation for the in-water electric and magnetic fields from a submerged HED in shallow water have been derived, with the solution given in [8.9]. Similarly, computing the fields for an HMD in the ocean requires both the horizontal and vertical magnetic Hertz vectors. The equations for the in-air electric and magnetic fields from submerged VED, HED, and HMD sources have been complied in [8.10], while the in-water fields from these three sources located above the ocean are summarized in [8.11]. The referenced shallow water equations can be reduced to the deep-ocean case by setting the bottom conductivity equal to that of the water.

Although the electromagnetic fields from dipole sources submerged in a deep ocean have been formulated in the generalized form of Sommerfeld integrals, it is very convenient to have algebraic equations readily accessible for obtaining quick estimates; even if they are only valid for special cases. The algebraic in-water and in-air electric and magnetic field equations for VED, HED, VMD, and HMD sources submerged in a deep ocean will be presented in tabular form for a few special cases. These tabularized equations have been found to be useful as a fast and easy reference.

The coordinate system and geometry for the tabulated equations are again shown in Fig. 8.10. All sources will be located at a depth h, with the VED and VMD aligned in the positive z direction, while the HED and HMD are oriented along the positive x-axis. The planner sea surface interface is at $z = 0$. The magnetic and electric dipole source strengths will be designated as m and p, respectively.

The magnetic and electric fields for static magnetic and electric dipoles in an unbounded ocean were given previously in spherical coordinates. At times, it is more convenient to apply the formulas in the Cartesian system. For easy reference, the Cartesian field equations for a static VMD and HMD source in an unbounded ocean (no sea surface) are listed in Table 8.1. Although static magnetic sources produce no electric fields, static VED and HED dipoles create both magnetic and electric fields as given in Table 8.2 for an unbounded ocean.

If the sea surface interface is now reintroduced at $z = 0$ (Fig. 8.10), the magnetic field equations for the static VMD and HMD sources in Table 8.1 remain unchanged. These equations are valid whether the observation point is in water, air, or sea bottom. The reason is that all three media are nonmagnetic with a permeability equal to that of free-space.

The jump in conductivity at the ocean's surface does, however, affect both the electric and magnetic fields from submerged electric dipoles. Because the air is nonconducting, the electric current in the conducting seawater will stay confined within it and will not flow across the surface interface. The sea surface is equivalent to an ideal reflector of static electric current. In addition, the discontinuity in the electric current across the surface interface produces additional components of magnetic fields.

Mathematically, the effects of the sea surface on the in-water static electric fields is equivalent to placing images of the VED and HED directly above the water at a distance equal to the depth of the sources. The electric fields produced by these images are listed in Table 8.3 [8.12]. To get the total in-water static electric fields for the deep ocean case, the VED and

Table 8.1 Static VMD and HMD sources located at (0, 0, h) in an unbounded ocean

	E_x	E_y	E_z	H_x	H_y	H_z
VMD	0	0	0	$\frac{3m_z x(z-h)}{4\pi r^5}$	$\frac{3m_z y(z-h)}{4\pi r^5}$	$\frac{m_z(2(z-h)^2-x^2-y^2)}{4\pi r^5}$
HMD	0	0	0	$\frac{m_x(2x^2-y^2-(z-h)^2)}{4\pi r^5}$	$\frac{3m_x xy}{4\pi r^5}$	$\frac{3m_x x(z-h)}{4\pi r^5}$

where $r=\sqrt{x^2+y^2+(z-h)^2}$

Table 8.2 Static VED and HED sources located at (0, 0, h) in an unbounded ocean

	E_x	E_y	E_z	H_x	H_y	H_z
VED	$\frac{3p_z x(z-h)}{4\pi\sigma r^5}$	$\frac{3p_z y(z-h)}{4\pi\sigma r^5}$	$\frac{p_z(2(z-h)^2-x^2-y^2)}{4\pi\sigma r^5}$	$\frac{-p_z y}{4\pi r^3}$	$\frac{p_z x}{4\pi r^3}$	0
HED	$\frac{p_x(2x^2-y^2-(z-h)^2)}{4\pi\sigma r^5}$	$\frac{3p_x xy}{4\pi\sigma r^5}$	$\frac{3p_x x(z-h)}{4\pi\sigma r^5}$	0	$\frac{-p_x(z-h)}{4\pi r^3}$	$\frac{p_x y}{4\pi r^3}$

where $r=\sqrt{x^2+y^2+(z-h)^2}$ and σ is the seawater conductivity

Table 8.3 In-water electric fields produced by the above-water images of submerged static VED and HED sources (after [8.12])

	E_x	E_y	E_z
VED	$\frac{-3p_z x(z+h)}{4\pi\sigma r_i^5}$	$\frac{-3p_z y(z+h)}{4\pi\sigma r_i^5}$	$\frac{-p_z(2(z+h)^2-x^2-y^2)}{4\pi\sigma r_i^5}$
HED	$\frac{p_x(2x^2-y^2-(z+h)^2)}{4\pi\sigma r_i^5}$	$\frac{3p_x xy}{4\pi\sigma r_i^5}$	$\frac{3p_x x(z+h)}{4\pi\sigma r_i^5}$

where $r_i=\sqrt{x^2+y^2+(z+h)^2}$ and σ is the seawater conductivity

Table 8.4 In-water magnetic fields produced by the above-water images of submerged static VED and HED sources (after [8.12])

	H_x	H_y	H_z
VED	$\frac{p_z y}{4\pi r_i^3}$	$\frac{-p_z x}{4\pi r_i^3}$	0
HED	$\frac{-p_x xy}{4\pi\rho^4}\left[2-\frac{(z+h)(2(z+h)^2+3\rho^2)}{r_i^3}\right]$	$\frac{p_x}{4\pi}\left\{\frac{x^2}{\rho^4}\left[2-\frac{(z+h)(2(z+h)^2+3\rho^2)}{r_i^3}\right]-\frac{1}{r_i^2+(z+h)r_i}\right\}$	0

where $r_i=\sqrt{x^2+y^2+(z+h)^2}$ and $\rho=\sqrt{x^2+y^2}$

Table 8.5 In-air electric fields from static VED and HED sources submerged at a depth h in a deep ocean (after [8.12])

	E_x	E_y	E_z
VED	$\frac{3p_z x(z-h)}{2\pi\sigma r^5}$	$\frac{3p_z y(z-h)}{2\pi\sigma r^5}$	$\frac{p_z(2(z-h)^2-x^2-y^2)}{2\pi\sigma r^5}$
HED	$\frac{p_x(2x^2-y^2-(z-h)^2)}{2\pi\sigma r^5}$	$\frac{3p_x xy}{2\pi\sigma r^5}$	$\frac{3p_x x(z-h)}{2\pi\sigma r^5}$

where $r=\sqrt{x^2+y^2+(z-h)^2}$ and σ is the seawater conductivity. Note: A negative value for z is used for in-air computations

HED equations in Table 8.3 must be added to their corresponding components from Table 8.2. Likewise, the magnetic field formulations produced by the jump in the surface current density has been computed in [8.12], and are listed in Table 8.4. Adding the equations in Table 8.4 to their corresponding magnetic

Table 8.6 In-air magnetic fields from static VED and HED sources submerged at a depth h in a deep ocean (after [8.12])

	H_x	H_y	H_z
VED	0	0	0
HED	$\frac{-p_z xy}{4\pi\rho^4}\left[2-\frac{(h-z)(2(h-z)^2+3\rho^2)}{r^3}\right]$	$\frac{-p_z}{4\pi}\left\{\frac{(z-h)}{r^3}+\frac{x^2}{\rho^4}\left[2-\frac{(h-z)(2(h-z)^2+3\rho^2)}{r^3}\right]-\frac{1}{r^2+(h-z)r}\right\}$	$\frac{p_x y}{4\pi r^3}$

where $r=\sqrt{x^2+y^2+(z-h)^2}$ Note: A negative value for z is used for in-air computations

Table 8.7 Electric field subsurface-to-subsurface propagation formulas for the quasi-static range, when $|\gamma_0\rho| \ll 1 \ll |\gamma\rho|$ and $\rho \gg h$ and z

	E_x	E_y	E_z
VED	$-\frac{p_z x}{2\pi\sigma\rho^3}\frac{\gamma_0^2}{\gamma}e^{-\gamma(z+h)}$	$\frac{p_z y}{2\pi\sigma\rho^3}\frac{\gamma_0^2}{\gamma}e^{-\gamma(z+h)}$	$\frac{p_z}{2\pi\sigma\rho^3}\frac{\gamma_0^2}{\gamma^2}e^{-\gamma(z+h)}$
VMD	$\frac{3m_z y}{2\pi\sigma\rho^5}e^{-\gamma(z+h)}$	$-\frac{3m_z x}{2\pi\sigma\rho^5}e^{-\gamma(z+h)}$	0
HED	$\frac{p_x}{2\pi\sigma\rho^5}(x^2-2y^2)e^{-\gamma(z+h)}$	$\frac{3p_x xy}{2\pi\sigma\rho^5}e^{-\gamma(z+h)}$	$\frac{p_x x}{2\pi\sigma\rho^3}\frac{\gamma_0^2}{\gamma^2}e^{-\gamma(z+h)}$
HMD	$-\frac{3m_x xy\gamma}{2\pi\sigma\rho^5}e^{-\gamma(z+h)}$	$-\frac{m_x\gamma}{2\pi\sigma\rho^5}(y^2-2x^2)e^{-\gamma(z+h)}$	$\frac{m_x y\gamma_0^2}{2\pi\sigma\rho^3}e^{-\gamma(z+h)}$

where $\rho=\sqrt{x^2+y^2}$ and σ is the seawater conductivity

Table 8.8 Magnetic field subsurface-to-subsurface propagation formulas for the quasi-static range, when $|\gamma_0\rho| \ll 1 \ll |\gamma\rho|$ and $\rho \gg h$ and z

	H_x	H_y	H_z
VED	$-\frac{p_z y}{2\pi\rho^3}\frac{\gamma_0^2}{\gamma^2}e^{-\gamma(z+h)}$	$-\frac{p_z x}{2\pi\rho^3}\frac{\gamma_0^2}{\gamma^2}e^{-\gamma(z+h)}$	0
VMD	$-\frac{3m_z x}{2\pi\gamma\rho^5}e^{-\gamma(z+h)}$	$-\frac{3m_z y}{2\pi\gamma\rho^5}e^{-\gamma(z+h)}$	$-\frac{9m_z}{2\pi\gamma^2\rho^5}e^{-\gamma(z+h)}$
HED	$\frac{3p_x xy}{2\pi\gamma\rho^5}e^{-\gamma(z+h)}$	$-\frac{p_x}{2\pi\gamma\rho^5}(x^2-2y^2)e^{-\gamma(z+h)}$	$\frac{3p_x y}{2\pi\gamma^2\rho^5}e^{-\gamma(z+h)}$
HMD	$-\frac{m_x}{2\pi\rho^5}(y^2-2x^2)e^{-\gamma(z+h)}$	$\frac{3m_x xy}{2\pi\rho^5}e^{-\gamma(z+h)}$	$\frac{3m_x x}{2\pi\gamma\rho^5}e^{-\gamma(z+h)}$

where $\rho=\sqrt{x^2+y^2}$ and σ is the seawater conductivity.

components in Table 8.2 yields the total in-water magnetic field for VED and HED sources submerged in a deep ocean.

For completeness, the equations for the total in-air electric fields from static VED and HED sources submerged in a deep ocean are listed in Table 8.5. The total in-air magnetic fields for the same case are found in Table 8.6. Tables 8.5 and 8.6 are the total in-air equations and are not added to any others. It should be noted that a negative value for z is to be used when computing the fields above the ocean surface. The deep ocean equations in Tables 8.3–8.6 were reduced from those found in [8.12] for a shallow sea.

The equations in Tables 8.1 through 8.6 apply for the special case where the sources are static or quasi-DC. They are valid for frequencies that correspond to seawater skin-depths that are large compared to the distance between the source and observation point, and their depths below the surface. At the other extreme, analytic equations have been formulated for the special case where the separation between the source and observation point is much greater than a seawater skin-depth and their depths. These equations were derived by taking the asymptotic limits for the Sommerfeld formulations.

The condition that the submerged source is many seawater skin-depths from the in-water observation point is equivalent to $1 \ll |\gamma\rho|$. In addition, if $\rho \gg h$ and z and the quasi-static range applies, $|\gamma_0\rho| \ll 1$, the subsurface-to-subsurface electric field equations in

Table 8.7 can be used for the four dipole types. The corresponding subsurface-to-subsurface magnetic field equations are listed in Table 8.8. These Cartesian formulations are re-arrangements of the cylindrical forms found in Table 3–16 of [8.13].

The propagation path described by the formulations in Tables 8.7 and 8.8 is quite unique. Since $1 \ll |\gamma\rho|$, the fields that travel directly from the source to the observation point or reflected off the sea-surface are significantly attenuated. Instead, the dominated propagation path is vertical to the surface, along the water–air interface, and then directly down to the observation point. The fields are attenuated in this *up-over-and-down* path only over the vertical distances between the source and surface, and from the surface to the observation point.

There are many other special cases in which analytic propagation equations can be used instead of numerically evaluating the Sommerfeld formulations. Many of the asymptotic conditions has been tabulated in [8.13]. In addition, the region between the quasi-DC and asymptotic conditions have been subdivided into ranges for which analytic formulations are been produced using *modified image theory* [8.14].

8.8 Electromagnetic Propagation in the Ocean at Optical Wavelengths

The electromagnetic constitutive parameters of seawater are not constant at microwave frequencies and higher. Indeed, if the nominal seawater ELF constitutive parameters are used to determine the electromagnetic attenuation at an optical frequency of visible blue–green light (6×10^{14} Hz), a value of 731 dB/m is computed. And yet, experimental measurements of blue–green light attenuation in clear seawater shows only 0.15 dB/m [8.15]. Obviously, the interaction of electromagnetic waves with the ocean at optical wavelengths is quite different than at low frequencies.

Although the physics of light transmission through seawater is quite involved, the discussion here will be at the engineering level, and confined to the *apparent optical properties* (AOP) of the ocean. The AOP for seawater is applicable to many problems in ocean engineering and, with the appropriate equipment, they can be measured in situ. Here, the in air optical wavelengths of interest cover the visible range from about 400 nm for violet colors to 700 nm for red.

The primary electromagnetic parameter of interest at optical wavelengths is the *specular irradiance*. The specular irradiance, designated by the term $E_{\lambda 0}$, is the band-limited power per unit area, with units of $\mathrm{W\,m^{-2}\,nm^{-1}}$. This is a measure of the scalar power density of an electromagnetic wave. The scalar power density or specular irradiance is proportional to the square of the electric or magnetic field presented in the previous sections of this chapter.

An important ocean engineering AOP is the attenuation coefficient for the specular irradiance as the light propagates through the sea. The equation describing the attenuation of optical irradiance from point r_1 to r is given by

$$E_{\lambda 0}(r) = E_{\lambda 0}(r_1)\mathrm{e}^{-\mathrm{K}_\lambda(\mathrm{r}-\mathrm{r}_1)}\,, \qquad (8.137)$$

where K_λ is the diffuse attenuation coefficient, which is a function of wavelength. Equation (8.137) is similar to that of a plane wave given in Sect. 8.3, and in fact, does not account for any spatial spreading of the light energy. The major difference is that (8.134) describes the attenuation of power instead of field amplitude, and the attenuation coefficient K_λ is quite different from the ELF values given previously for the field attenuation constant α.

The optical diffuse attenuation coefficient is a function of wavelength, and is comprised of two major components that contribute to its overall value: absorption and scattering. Although there is absorption of light due to the intrinsic or inherent properties of clear seawater, other optical absorption mechanisms found in the ocean include organic materials such as chlorophylls in phytoplankton and dissolved organic compounds called *yellow substance* or *Gelbstoffe*. In addition, the small wavelength of visible light will cause it to scatter off organic and inorganic particulates suspended in the water, adding to its attenuation. As would be expected, the optical attenuation coefficient varies with

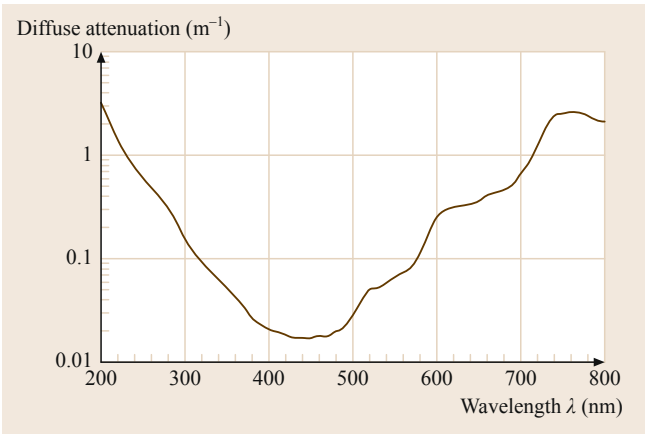

Fig. 8.11 Diffuse attenuation coefficient for clear seawater (after [8.16])

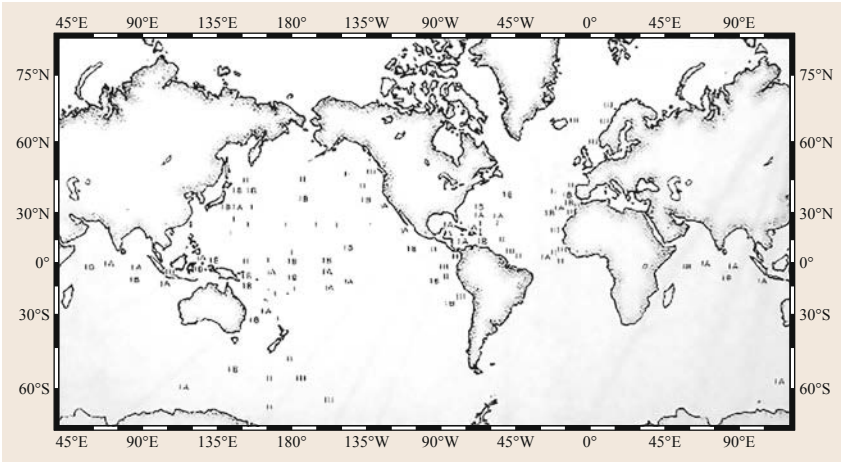

Fig. 8.12 The global distribution of Jerlov water types (after [8.1])

depth and between different regions of the world's oceans.

Laboratory measurements of the attenuation, absorption, and scattering coefficients of pure or clear seawater have been reviewed and tabulated [8.16]. The diffuse attenuation coefficients in pure seawater are plotted in Fig. 8.11, and includes water absorption and a small amount of scattering from sea salts. The estimated accuracy of this data is reported to be within +25 and −5% for wavelengths between 300 and 480 nm, and 10 and 5% from 480 to 800 nm. Below 300 nm the data is considered to be no better than an *educated estimate* [8.16]. The region of minimum attenuation between 400 and 500 nm is called the blue–green window, and has been the subject of many investigations to engineer underwater communication and detection systems [8.15, 18].

The seminal work of Jerlov produced a classification method for characterizing the optical properties of the world's oceans. Based on the measured irradiance transmissivity in the upper 10 m of the water, the oceans are categorized as Type I to III, with a subsequent subdivision of Type I into IA and IB. Coastal waters are divided into types ranging from 1 to 9. These water clarity classifications account not only for the absorption and scattering of pure seawater, but also included the effects of the suspended organic and inorganic particles as described above. A map of the global distribution of Jerlov water types is shown in Fig. 8.12 [8.1, p. 584].

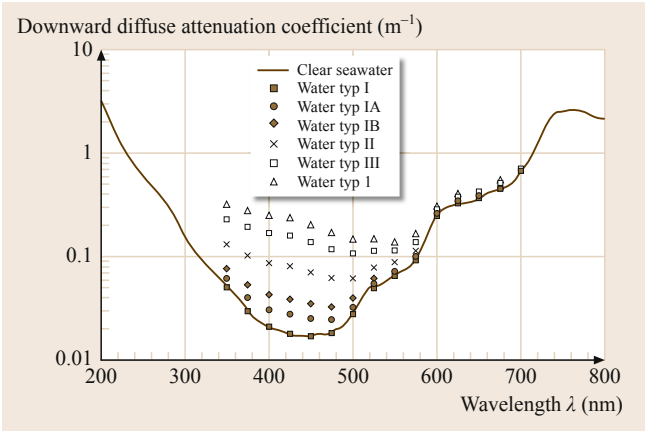

Fig. 8.13 Diffuse attenuation coefficient for Jerlov water types (after [8.17])

The downward looking diffuse attenuation coefficients for some of the Jerlov water types have been measured and tabulated [8.17]. The attenuation coefficients for ocean water Types I though III and coastal Type 1 are plotted in Fig. 8.13. As expected, the attenuation coefficient increases as water clarity decrease, with the minimum in the optical window moving toward longer wavelengths. The higher attenuation of light in natural seawaters, especially for coastal regions, limits the useful ranges of communication and detection systems that are based on blue–green lasers.

Although the dielectric constant of seawater is approximately 80 up through the ELF band, its value at an optical wavelength of 700 nm is only 1.79 at 20 °C, and increases to only 1.83 for 400 nm at 4 °C at the other extreme [8.1, pp. 532–539]. A nominal value of 1.8 gives a propagation constant of $\beta \approx 1.4 \times 10^7$ rad/m at 450 nm (20 °C), while the equivalent field attenuation constant for pure seawater is estimated from K_λ to be $\alpha \approx 0.008$ Np/m at this wavelength. Therefore, seawater can be considered a dielectric at optical wavelengths, with an average index of refraction of $n \approx 4/3$ ($n = \sqrt{\varepsilon_w}$). The index of refraction is the ratio of the speed of light in air, 3×10^8 m/s, to that in seawater, 2.24×10^8 m/s.

Since seawater can be treated as a dielectric at optical wavelengths, the expressions for the field reflection and transmission coefficients given previously for fresh

water can also be used for the ocean. The only difference is that they must be squared before applying them to irradiance, which is power. The power reflection coefficients for perpendicular $R_\perp$ and parallel polarization $R_\parallel$ can be obtained from (8.59) and (8.71), giving

$$R_\perp = \Gamma_\perp^2 = \frac{\tan^2(\theta_\mathrm{i} - \theta_\mathrm{t})}{\tan^2(\theta_\mathrm{i} + \theta_\mathrm{t})} \,, \tag{8.138}$$

$$R_\parallel = \Gamma_\parallel^2 = \frac{\sin^2(\theta_\mathrm{i} - \theta_\mathrm{t})}{\sin^2(\theta_\mathrm{i} + \theta_\mathrm{t})} \,, \tag{8.139}$$

and

$$\theta_\mathrm{r} = \theta_\mathrm{i} \,, \tag{8.140a}$$

$$\sin\theta_\mathrm{i} = n \sin\theta_\mathrm{t} \,. \tag{8.140b}$$

where all terms have been defined previously. The Brewster angle can be computed directly from $\tan\theta_\mathrm{B} = n$. These equations are valid for a smooth surface. A discussion of optical scattering from a rough ocean surface produced by wind waves can be found in [8.1, p. 528].

The maximum refraction angle of light into the ocean is limited. If the incidence angle of light entering the flat surface of the sea approaches the grazing angle ($\theta_\mathrm{i} = 90°$), then from (8.140b) the transmission angle of the refracted light is computed to be approximately 48.6°. This means that all images from the entire hemisphere above water is funneled into an upward looking cone whose sides are 48.6° from the vertical. Any image that is seen at an angle greater than this could only be coming from a submerged object.

References

8.1 J.R. Apel: *Principles of Ocean Physics* (Academic Press, San Diego 1987)

8.2 C.A. Balanis: *Advanced Engineering Electromagnetics*, 2nd edn. (Wiley, Hoboken 2012)

8.3 C.A. Balanis: *Antenna Theory*, 3rd edn. (Wiley, Hoboken 2005) pp. 133–142

8.4 J. Mosig: The weighted averages algorithm revisited, IEEE Trans. Antennas Propag. **60**(4), 2011–2018 (2012)

8.5 J.R. Wait: Electromagnetic Fields of Sources in Lossy Media. In: *Antenna Theory*, ed. by R.E. Collin, F.J. Zucker (McGraw-Hill, New York 1969) pp. 476–478

8.6 A.C. Fraser-Smith, D.M. Bubenik: ULF/ELF electromagnetic fields generated above a sea of finite depth by a submerged vertically-directed harmonic magnetic dipole, Radio Sci. **14**, 59–74 (1979)

8.7 D.M. Bubenik, A.C. Fraser-Smith: ULF/ELF electromagnetic fields generated in a sea of finite depth by a submerged vertically-directed harmonic magnetic dipole, Radio Sci. **13**, 1011–1020 (1978)

8.8 J.R. Wait: *Electromagnetic Waves in Stratified Media* (IEEE Press, Piscataway 1996) pp. 143–146

8.9 C. Liu, L.G. Zheng, Y.P. Li: Study of ELF electromagnetic fields from a submerged horizontal electric dipole positioned in a sea of finite depth, IEEE 3rd Int. Symp. Microw. Antenna Propag. EMC Technol. Wirel. Commun. (2009) pp. 152–157

8.10 A.C. Fraser-Smith, D.M. Bubenik: *Compendium of the ULF/ELF Electromagnetic Fields Generated Above a Sea of Finite Depth by Submerged Harmonic Dipoles*, Tech. Rep., Vol. E715-1 (Stanford Univ., Stanford 1980)

8.11 A.C. Fraser-Smith, D.M. Bubenik: *ULF/ELF/VLF Electromagnetic Fields Generated in a Sea of Finite Depth by Elevated Dipole Sources*, Tech. Rep., Vol. E715-2 (Stanford Univ., Stanford 1984)

8.12 D.L. Jones, C.P. Burke: The DC field components of horizontal and vertical electric dipole sources immersed in three-layer stratified media, Ann. Geophys. **15**, 503–510 (1997)

8.13 M.B. Kraichman: Electromagnetic propagation in conducting media. In: *Electromagnetics Problem Solver*, ed. by M. Fogiel (REA, Piscataway 2000) pp. 3–24, Section II

8.14 P.R. Bannister, R.L. Dube: Simple expressions for horizontal electric dipole quasi-static range subsurface-to-subsurface and subsurface-to-air propagation, Radio Sci. **13**(3), 501–507 (1978)

8.15 W.C. Cox: A 1 Mbps Underwater Communication System Using a 405 nm Laser Diode and Photomultiplier Tube, Master Thesis (North Carolina State Univ., Raleigh 2007)

8.16 R.C. Smith, K.S. Baker: Optical properties of the clearest natural waters (200–800 nm), Appl. Opt. **20**(2), 177–184 (1971)

8.17 R.W. Austin, T.J. Petzold: Spectral dependence of the diffuse attenuation coefficient of light in ocean waters, Opt. Engr. **25**, 471 (1986)

8.18 C.J. Cassidy: Airborne Laser Mine Detection System, Master Thesis (Naval Postgraduate School, Monterey 1995)